Author Manuscript

Author Manuscript

Author Manuscript

Author Manuscript

HHS Public Access

Author manuscript

Chromosome Res. Author manuscript; available in PMC 2015 July 14.

Published in final edited form as:

Chromosome Res. 2015 June ; 23(2): 311–331. doi:10.1007/s10577-015-9471-y.

Canine urothelial carcinoma: genomically aberrant and comparatively relevant

S. G. Shapiro,
Department of Molecular Biomedical Sciences, College of Veterinary Medicine, North Carolina State University, 1060 William Moore Drive, Raleigh, NC 27607, USA

S. Raghunath,
Department of Molecular Biomedical Sciences, College of Veterinary Medicine, North Carolina State University, 1060 William Moore Drive, Raleigh, NC 27607, USA; Department of Pediatrics and Huntsman Cancer Institute, University of Utah, 2000 Circle of Hope, Salt Lake City, UT 84112, USA

C. Williams,
Department of Molecular Biomedical Sciences, College of Veterinary Medicine, North Carolina State University, 1060 William Moore Drive, Raleigh, NC 27607, USA

A. A. Motsinger-Reif,
Department of Statistics, College of Sciences, North Carolina State University, Raleigh, NC, USA; Center for Comparative Medicine and Translational Research, North Carolina State University, Raleigh, NC, USA

J. M. Cullen,
Department of Population Health and Pathobiology, College of Veterinary Medicine, North Carolina State University, Raleigh, NC, USA; Center for Comparative Medicine and Translational Research, North Carolina State University, Raleigh, NC, USA

T. Liu,
Anatomic Pathology Division Department of Pathology, University of Utah, 1950 Circle of Hope, RM N3105, Salt Lake City, UT 84112, USA

D. Albertson,
Anatomic Pathology Division Department of Pathology, University of Utah, 1950 Circle of Hope, RM N3105, Salt Lake City, UT 84112, USA

M. Ruvolo,
Agilent Technologies, 5301 Stevens Creek Blvd., Santa Clara, CA 95051, USA

A. Bergstrom Lucas,
Agilent Technologies, 5301 Stevens Creek Blvd., Santa Clara, CA 95051, USA

J. Jin,
Agilent Technologies, 5301 Stevens Creek Blvd., Santa Clara, CA 95051, USA

Correspondence to: M. Breen, Matthew_Breen@ncsu.edu.

Electronic supplementary material The online version of this article (doi:10.1007/s10577-015-9471-y) contains supplementary material, which is available to authorized users.

Author Manuscript Author Manuscript Author Manuscript Author Manuscript

D. W. Knapp,
Department of Veterinary Clinical Sciences, Purdue University, School of Veterinary Medicine, West Lafayette, IN, USA

J. D. Schiffman, and
Department of Pediatrics and Huntsman Cancer Institute, University of Utah, 2000 Circle of Hope, Salt Lake City, UT 84112, USA

M. Breen
Department of Molecular Biomedical Sciences, College of Veterinary Medicine, North Carolina State University, 1060 William Moore Drive, Raleigh, NC 27607, USA; Center for Comparative Medicine and Translational Research, North Carolina State University, Raleigh, NC, USA; Center for Human Health and the Environment, North Carolina State University, Raleigh, NC, USA; Lineberger Comprehensive Cancer Center, University of North Carolina, Chapel Hill, NC, USA

M. Breen: Matthew_Breen@ncsu.edu

Abstract

Urothelial carcinoma (UC), also referred to as transitional cell carcinoma (TCC), is the most common bladder malignancy in both human and canine populations. In human UC, numerous studies have demonstrated the prevalence of chromosomal imbalances. Although the histopathology of the disease is similar in both species, studies evaluating the genomic profile of canine UC are lacking, limiting the discovery of key comparative molecular markers associated with driving UC pathogenesis. In the present study, we evaluated 31 primary canine UC biopsies by oligonucleotide array comparative genomic hybridization (oaCGH). Results highlighted the presence of three highly recurrent numerical aberrations: gain of dog chromosome (CFA) 13 and 36 and loss of CFA 19. Regional gains of CFA 13 and 36 were present in 97% and 84% of cases, respectively, and losses on CFA 19 were present in 77% of cases. Fluorescence in situ hybridization (FISH), using targeted bacterial artificial chromosome (BAC) clones and custom Agilent SureFISH probes, was performed to detect and quantify these regions in paraffin-embedded biopsy sections and urine-derived urothelial cells. The data indicate that these three aberrations are potentially diagnostic of UC. Comparison of our canine oaCGH data with that of 285 human cases identified a series of shared copy number aberrations. Using an informatics approach to interrogate the frequency of copy number aberrations across both species, we identified those that had the highest joint probability of association with UC. The most significant joint region contained the gene *PABPC1*, which should be considered further for its role in UC progression. In addition, cross-species filtering of genome-wide copy number data highlighted several genes as high-profile candidates for further analysis, including *CDKN2A*, *S100A8/9*, and *LRP1B*. We propose that these common aberrations are indicative of an evolutionarily conserved mechanism of pathogenesis and harbor genes key to urothelial neoplasia, warranting investigation for diagnostic, prognostic, and therapeutic applications.

Keywords

Canine; Urothelial carcinoma; Transitional cell carcinoma; Cytogenetics; Chromosome aberration; Array comparative genomic hybridization; Comparative oncology

Author Manuscript Author Manuscript Author Manuscript Author Manuscript

Introduction

Urothelial carcinoma (UC) of the bladder, also known as transitional cell carcinoma (TCC), is the second most common human urogenital cancer, surpassed only by prostate cancer. In 2014, an estimated 74,690 UC diagnoses were made in the USA alone, comprising 4–5% of all human cancer diagnoses (American Cancer Society 2014). Similarly, UC is the most common urogenital cancer of dogs, representing 1.5–2% of canine cancer diagnoses annually in the USA (Mutsaers et al. 2003; Oliveira et al. 2014). At diagnosis, approximately 20% of canine and 10% of human patients have overt metastasis, with microscopic metastases likely present in many more cases (Knapp et al. 2000; Oliveira et al. 2014). Due to the high metastatic rate and, particularly in canines, delayed diagnosis, the identification of potential early diagnostic indicators, including genomic changes, is highly desirable.

Previous studies have established that canine UC resembles and behaves similarly to invasive human UC, providing a beneficial in vivo model for the disease (Knapp et al. 2000; Dhawan et al. 2009). The canine cancer model is an optimal one for human cancers: people and their pets share an environment, have similar relative life spans, and develop the disease naturally (Shearin and Ostrander 2010). Additionally, bottlenecks in the domestic dog population due to tightly controlled breeding have created breeds of dogs with high genetic similarity and resultant disease predispositions (Dobson 2013). Scottish Terriers are 20 times more likely to develop UC than the average dog (Knapp et al. 2014). Other breeds with high incidence of UC include Shetland Sheepdogs, Beagles, West Highland White Terriers, and Wire Hair Fox Terriers, who are three to five times more likely to develop UC than the general dog population. The overwhelming breed predispositions associated with canine UC suggest a strong genetic component to disease development. Interspecies chromosome syntenty allows us to capitalize on the unique genetic homogeneity of purebred dogs to elucidate more specific, evolutionarily conserved, and relevant genomic aberrations in humans, regions that may prove clinically relevant to both dogs and people.

In the current study, we evaluated 31 primary canine UC tumor biopsies via genome-wide oligonucleotide array comparative genomic hybridization (oaCGH). Validation of CGH data was performed using formalin fixed paraffin-embedded (FFPE) UC biopsies (n=5) and urine sediments (n=24) via fluorescence in situ hybridization (FISH). A hematoxylin and eosin (H&E)-stained slide of each tumor biopsy was evaluated and staged in parallel by human and veterinary pathologists. Canine oaCGH data were compared with those derived from 285 UCs, revealing striking similarities of copy number gains and losses shared between species. Additionally, we describe a high-specificity FISH-based method for canine UC diagnosis utilizing low-volume, free-catch urine specimens. These data suggest: (1) the diagnostic relevance of genomic aberrations in veterinary medicine, (2) a non-invasive method of canine UC diagnosis, and (3) the canine model is a valuable model in the study of human UC.

Author Manuscript Author Manuscript Author Manuscript Author Manuscript

Methods and materials

Canine UC case collection

Cystoscopy or cytstotomy specimens were obtained from a series of chemotherapy-naïve, client-owned dogs presenting with suspected UC at the veterinary hospitals at Purdue University (PU) and North Carolina State University (NCSU). Each biopsy specimen was either snap frozen and subsequently stored in liquid nitrogen, or fixed in 10% neutral buffered formalin (NBF) for 24 h prior to embedding in paraffin. Histopathological evaluation confirmed a diagnosis of UC for all 31 specimens (Table 1). Urine samples (n=24) were collected via free catch (1–5 mL) from additional NCSU patients with confirmed UC (diagnosis via urine cytology or histopathology) and stored at 4°C for a maximum of 24 h until further processing (see below). Control urothelium was collected from recently euthanized dogs at necropsy and confirmed to be non-neoplastic by histopathologic evaluation. All biopsy and urine specimens were obtained with informed client consent and under institutionally approved protocols at PU and NCSU.

Pathologic evaluation of canine UC

H&E-stained slides previously used for canine UC diagnosis were reviewed by a board-certified veterinary pathologist (JC) and two human genitourinary pathologists (TL, DA). Slides were first scanned at low magnification to locate the neoplastic regions of the biopsy. Magnification was then increased to allow identification of specific histologic criteria in the neoplasms. The urothelial basement membrane was evaluated for evidence of invasion, as shown by a clear breech in basement membrane and invasion of the lamina propria of the bladder (stage T1). If no such invasion was observed, tumors were classified as either Ta (papillary carcinoma) or Tis (in situ “flat tumor”). When the biopsy included deeper layers of the bladder wall, the UC was graded on the basis of the extent of invasion of the bladder. UC that invaded the muscularis propria were graded as T2, and those that extended into the perivesical tissues were graded as T3. Pathologic staging was performed in accordance with the World Health Organization (WHO) and American Joint Committee on Cancer (AJCC) guidelines (American Joint Committee on Cancer 2002). The compiled pathologic data are included in Table 1.

Canine oaCGH

DNA was extracted from biopsy specimens using either the DNeasy Kit (frozen samples, Qiagen, Valencia, CA) or QIAamp DNA FFPE Tissue Kit (FFPE samples, Qiagen). DNA samples were verified to be of sufficient quantity and integrity by agarose gel electrophoresis (>1 kb) and spectrophotometry (260:280 and 260:230 both >1.8). Gender-specific DNA reference samples were generated from whole blood of healthy mixed-breed dogs, pooling equimolar quantities of DNA from ten males or ten females. DNA was labeled using the Genomic DNA Enzymatic Labeling Kit (Agilent, Santa Clara, CA), as described previously (Poorman et al. 2014; Thomas et al. 2014). Fluorescently labeled test and reference samples were hybridized to Canine G3 SurePrint 180,000 feature oaCGH arrays (Agilent, AMADID 025522) for 40 h, as described previously (Poorman et al. 2014; Thomas et al. 2014). Arrays were scanned at 3 μm (Agilent, Model G2505C); data were extracted using Feature Extraction v10.10 software (Agilent Technologies, Santa Clara, CA)

Author Manuscript Author Manuscript Author Manuscript Author Manuscript

and assessed for quality using the Quality Metrics report tool in Agilent's Feature extraction software (v10.5) (Agilent Technologies). Raw data were evaluated to identify and exclude probes displaying non-uniform hybridization or signal saturation and imported into Nexus copy number v7.5 (BioDiscovery, Hawthorne, CA) for analysis. Copy number calls were made using the FASST2 segmentation algorithm with a significance threshold of 5.05^{-6}. Aberrations were defined as a minimum of three consecutive probes with log2 tumor: reference value of >1.14 (high gain), 1.13 to 0.201 (gain), −0.234 to −1.1 (loss), and ≤1.1 (big loss).

Selection of canine diagnostic regions

Genome-wide oaCGH data for the canine cohort were evaluated to identify chromosomal regions that exhibited the highest penetrance of aberrations. To develop a DNA copy number-based assay for the detection of neoplastic epithelial transitional cells shed in the urine, three regions with the highest frequency of unidirectional aberration in neoplastic biopsies were identified and compared with oaCGH data from a cohort of 100 non-neoplastic DNA specimens. Aberrant regions were classified as gains, losses, or neutral for the purposes of classification. Potential predictive model(s) were built using the classification tree algorithm J48, as implemented in Weka c3.7 (Hall et al. 2009). The J48 algorithm was implemented both with and without fivefold cross-validation, in order to assess the potential predictive performance. In both cases, the same model (in terms of variables selected and tree architecture) resulted, so only the model without cross-validation is presented here (for simplicity). Several measures of model fit were calculated, including the relative risk, odds ratio, sensitivity, specificity, and overall misclassification rate for each of the three regions.

Fluorescence in situ hybridization of canine FFPE biopsies using BAC and custom SureFISH probes

To validate oaCGH data, regions on CFA 13, 19, and 36 with >75% aberration frequency among patients and one balanced region on CFA 8 (oaCGH Log2=0 in 100% of patients) were selected for FISH analysis. Differentially labeled FISH probes for each of these four regions were generated using DNA isolated from canine bacterial artificial chromosome (BAC) clones of the CHORI-82 canine BAC library (http://bacpac.chori.org/library.php?id=253)(Table 2). In addition, in silico-selected sequences from non-repetitive canine genomic sequences (canfam2) were selected for the three unbalanced regions (segments of on CFA 13, 19, and 36) (Table 2) and submitted for massively parallel de novo synthesis and generation of custom SureFISH probes (Agilent Technologies), labeled with one of the three current color options (red, green, or aqua). Each FISH probe was first assessed to verify a unique cytogenetic location when hybridized to canine metaphase spreads and interphase nuclei from healthy dogs using protocols reported previously for BACs (Poorman et al. 2014) and per the manufacturer's recommendations for SureFISH probes (Agilent Technologies).

FISH was performed on 5 μm sections of FFPE biopsy specimens from healthy canine urothelium and from pathologically confirmed cases of UC, using protocols reported previously (Poorman et al. 2014; Thomas et al. 2014), with modifications. After

Author Manuscript Author Manuscript Author Manuscript Author Manuscript

deparaffinization with xylene treatment, slides were exposed to Hyaluronidase VIII (45 U/μL in 250 mM TRIS-buffered saline, pH 7.4, Sigma-Aldrich, St. Louis, MO) at 37°C for 1 h, followed by a combined collagenase treatment (236 U/μL each of collagenases I and II, and 0.4 U/μL of collagenase III (Invitrogen/Life Technologies, Carlsbad)) in HBSS with 2.4 mM $CaCl_2$ and pretreatment in 80°C sodium thiocyanate for 60 min. Slides were rinsed in MQ water, briefly dried, and then immersed in Abbott Protease II solution (Abbott Laboratories, Chicago, IL) for 45 min at 37°C. Pretreated slides were dehydrated through an ethanol series (70, 90, 100 %), and fluorescent probe (100 ng of each BAC or SureFISH probe) in hybridization solution was added. Probes and DNA were codenatured at 80°C for 5 min, followed by overnight hybridization at 37°C. All hybridization steps and post-hybridization washes and imaging were as described previously (Thomas et al. 2014). For each specimen, probes were visualized by mulitplane fluorescence microscopy, using a BioView imaging system built around an Olympus BX61. Probe signals were enumerated in >50 cells, each classified as aberrant or nor aberrant, and mean copy number per cell also obtained.

FISH of urine sediment

Free-catch urine was mixed with an equal volume of 1× phosphate-buffered saline (PBS) and exfoliated cells concentrated by centrifugation (1500 RPM). Urine sediment was rinsed in 10 mL 1× PBS. Following centrifugation, supernatant was aspirated to approximately 1 mL, the cells resuspended and fixed three times in 3:1 methanol/glacial acetic acid. The concentrated fixed cell suspension was spotted onto a glass slide for FISH analysis. Slides were dehydrated in an ethanol series (70/90/100 %) prior to being heated for 2 min at 65°C, transferred to a 37°C slide moat, and treated with pepsin solution for enzyme-induced epitope retrieval (Thermo Fisher Scientific, Cheshire, UK) for 30 s to eliminate signal background due to protein. Slides were rinsed twice in water and then fixed in 3:1 methanol/glacial acetic acid for 5 min, rinsed twice in water, and passed through a second dehydration series. Hybridization, washes, and imaging were as for the FFPE FISH.

Human oaCGH data

oaCGH-segmented data from 205 human urothelial tumors were accessed via the Cancer Genome Atlas (TCGA). Affymetrix Oncoscan FFPE Express Platform (Santa Clara, CA) data for an additional 80 cases were downloaded from Gene Expression Omnibus (GEO), GSE44323 (Karolchik et al. 2004; Chekaluk et al. 2013). Both data sets were imported and merged into a single project using Nexus copy number v7.5 (BioDiscovery, CA).

Humanization of canine oaCGH data for comparative analysis

Canine oaCGH data were recoded into “virtual” human genome format as described previously (Thomas et al. 2011; Poorman et al. 2014). Using these recoded coordinates, the tumor/reference signal intensity data for each canine data set were reprocessed to output the oaCGH profile according to their virtual human chromosome locations. All human and humanized canine data were imported into a single experiment in Nexus copy number v7.5 to allow a direct comparative analysis.

Author Manuscript Author Manuscript Author Manuscript Author Manuscript

Generation of call data and probe median values for comparative assessment

Raw data (log2 ratios) for the 80 human oaCGH profiles deposited in GEO and the 31 canine profiles generated in the current study were analyzed separately to generate species-specific lists of aggregate genome regions where DNA copy number aberrations (CNAs) were evident in >5% of the cohort. The TGCA data set was not associated with raw data values and so excluded from this component of the analysis. Regions with contiguous CNAs were selected, and the probe median values for each region calculated. Overlap analysis of the raw data sets was then performed to isolate regions of sequence similarity that have shared aberrations between canine and human data sets. The probe median values for each aggregate region for human and canine data were calculated and used to visualize the data as concentric Circos plots.

Isolation of regions of overlapping copy number aberration

For isolating regions of CNA shared between human and dog, two input files were created for each species: a reference file and a file containing aberration call data. The reference file contained syntenic regions of canine and human chromosomes, where each syntenic region was indexed using a “link ID” to identify the region throughout aberration analysis. The *intersect* option in Bedtools was used to first find intersecting regions between the aberration call data and the reference file for both the dog and human, using a threshold of 1 Mb (Quinlan and Hall 2010). The output was a list of overlapping aberrant regions between the canine and human data sets as mapped to the reference file. These aberrant regions were then matched to the respective link IDs between the two organisms, yielding a set of syntenic genomic regions sharing copy number loss or gain. Finally, overlapping link IDs were mapped to chromosomal regions with aberration calls, and the frequency of the specific aberration per species was calculated. Output data from the final step were merged to create a single file referenced by the link ID. Following this unsupervised analysis, the process was repeated to target seven a priori human bladder cancer-associated genes: *PPARG, EGFR, CCND1, MDM2, E2F3, CDKN2A*, and *RB1* (The Cancer Genome Atlas Research Network 2014), to provide verification that these genes also play a role in canine UC and suggest a shared pathogenesis.

Statistical validation of the gene list

Regions of conserved copy number aberrations between dog and human were extracted, ranked (using R) independently for each organism (based on the frequency) giving priority to regions of higher frequency, and validated by calculating the joint probability. For regions that tied for the same rank, the *ties.method* argument of R's rank function was used (R Development Team 2010). After calculating the individual ranks for human and dog aberrations, the maximum rank between dogs and humans was calculated, focusing on regions ranked highest in both species. The probability of the ranks for both gains and losses for each organism was calculated and the joint probability derived by multiplying the probabilities across both species. Regions with a nominally significant joint probability (<0.05) were further assessed.

Author Manuscript Author Manuscript Author Manuscript Author Manuscript

Comparative pathologic staging analysis

Comparative analysis was performed using all human (*n*=285) and canine (*n*=31) samples included in the genome-wide copy number analysis. Canine staging, performed as described above, resulted in two tumor groups: group A—Tis and T1, representing non-muscle invasive tumors, and group B—T2 and T3, representing muscle invasive tumors. Human cases were similarly grouped to allow a comparative analysis of the frequencies of CNAs identified across the two groups.

Results

Canine UC biopsies show recurrent DNA copy number aberrations

oaCGH data of DNA isolated from canine UC biopsy specimens revealed that all cases presented with numerous recurrent CNAs. Representative genome-wide profiles copy number are provided in Fig. 1. In all cases, the CNAs detected were primarily either whole chromosome or large segmental aneuploidy. In addition, there were one or more chromothriptic-like events detected in 74% (23/31) of patients involving 21 chromosomes. A chromothriptic-like event was defined as a cluster of sub-chromosomal regions showing alternating copy number gains and losses (Cai et al. 2014). An example of chromothriptic events in a single patient is shown in Fig. 2. While most occurred sporadically throughout the genome, chromothriptic-like events of CFA 36 were evident in almost 30% of the cohort, with involvement of CFA 10 and 16 at 16% and 13 %, respectively, and CFA 4 and 7 approaching 10% (Fig. 3). Assessment of the evolutionarily conserved chromosome segments (ECCS) of these five chromosome segments in the human data indicated that while chromothriptic-like events in the ECCS shared with CFA 36 were evident in only 1% of cases, such events involving genome regions conserved with CFA4, 7, 10, and 16 were detected in 5–7% of cases.

FASST2-processed oaCGH data were compiled into two penetrance plots representing the frequencies of called aberrations detected among the DNA samples derived from the fresh frozen and fixed tissue specimens (data not shown). Evaluation of the two data sets using the “compare” tool of Nexus indicated a high degree of concordance of the specimen type; only six aberrations >100 kb in size differed significantly in their frequencies between the two sample types. The size of these six regions ranged from 103–330 kb (mean=200 kb) and totaled just 1.2 Mb of the genome. With a high degree of concordance between the two specimen types, a penetrance plot representing aberration frequencies of all 31 cases of canine UC was generated (Fig. 4).

The highest frequency CNAs (>75% of cases) involved large segmented regions of CFA 13 (gain), 19 (loss), and 36 (gain) (Fig. 4). A second tier of recurrent copy number changes (frequency >33 %) was evident as copy number loss of regions of CFA 2, 5, 6, 10, 12, 26, 27, 28, and X and copy number gains involving regions of CFA 2, 4, 5, 6, 7, 10, 14, 17, 20, 23, 24, 30, 31, 35, 38, and X. A 1-Mb region located in CFA 8q12 represented a segment of the canine genome where no detectable copy changes were evident across the cohort and may thus be regarded as an indicator of copy number neutrality for assessment of ploidy status. Several highly penetrant gains or losses also exhibited subtle copy number changes in

Author Manuscript Author Manuscript Author Manuscript Author Manuscript

the opposing direction. To develop the most sensitive FISH-based assay designed to detect and quantify single loci, regions for probe selection were therefore based on those with unidirectional CNAs. The peaks of unidirectional aberration on CFA 13, 19, and 36 had frequencies of 96.77% gain, 77.42% loss, and 83.87% gain, respectively (Table 3). Evaluation of individual cases indicated that a region of CFA 36 was the most notably aberrant with Log2 ratios approaching 5.0 in several cases, suggesting genomic amplification.

FISH analysis of FFPE tumor biopsies and urine sediment allows direct visualization of urothelial cell copy number status

FISH analysis was performed in 5 μm sections of FFPE non-neoplastic (control) canine bladder specimens (n= 5). Currently, SureFISH probes are only available in three colors, limiting our analysis to only the aberrant target regions on CFA 13, 19, and 36. There was high concordance between data obtained from BAC and SureFISH probes; though the SureFISH probes were cleaner (had no visible background signal), had reduced variation and a marginally higher mean copy number (Fig. 5a). It is apparent from these data that the mean copy number of all probes tested was close to n=2 but slightly elevated (n=2.15–2.3). In most tissue types, the use of 5 μm sections results in degree of nuclear truncation, leading to a mean copy number of n<2. The elevated mean values in bladder epithelium are to be expected due to the presence of binucleate and/or tetraploid transitional epithelial cells, common even in healthy urothelium (Sahrief et al. 1980).

Both probe sets were used to assess copy number status of the target loci in cells obtained from FFPE UC tumor biopsies (n=5) previously interrogated by oaCGH (Fig. 5b). In each case, the data confirmed copy number gain of CFA 13 and 36 and loss of CFA 19 as recurrent features, with subtle differences in enumeration between BAC and SureFISH probes. In individual cells, the locus on CFA 36 was often detected as >8 copies/cell, and the mean of all individual patient means was ∼4.7. CFA 13 displayed more conservative copy number gains (mean=∼3.72), and CFA 19 was present in one to three copies (mean=∼2.2), depending on genome ploidy (Fig. 5b). The data from BAC and SureFISH probe sets were highly effective as a means to acquire enumeration data for all target loci. When used to probe transitional cells recovered from the urine sediment of UC patients (n=24), each case revealed the presence of one or more of the three target aberrations. The distribution of the mean copy numbers derived for each FISH probe along with the combined mean of all cases is presented in Fig. 5c, demonstrating the recurrent gain of CFA 13 and 36 and loss of CFA 19 detected by both BAC and SureFISH probes.

Copy number changes in canine UC—an aid to diagnosis

Analysis of DNA samples from pathologically verified non-neoplastic DNA samples (n=100) indicated normal copy number status (n=2) for each of CFA 13, 19, and 36. As such, the sensitivity, specificity, percent correctly classified, and the AUC values (with 95% CI) for each of the three regions were calculated, based on their aberration frequency in confirmed canine UC and the lack of detectable aberration in 100 non-neoplastic tissues. The measures of association and potential predictive performance calculated for each of three aberrations are presented in Table 4. To evaluate the potential predictive power of a

Author Manuscript Author Manuscript Author Manuscript Author Manuscript

multivariate model (using up to all three regions together, with gain and loss information for all three regions included), a decision tree model was constructed. With or without cross-validation, the best tree only had a single variable included, copy number gain of CFA 13. This was the best model and adding the additional variables neither improved nor weakened the model. In addition, if two or more of these three aberrations are detected in cells from a urinary tract specimen, the sensitivity and specificity to indicate the presence of neoplasm is extremely high (>99 %, based on the data set evaluated).

Canine and human urothelial tumors share copy number aberrations

The segmented canine oaCGH data were humanized to allow direct gross genome-wide comparison of CNA penetrance with accessible human segmented data (Fig. 6). While the general directional pattern of CNA penetrance across the genomes of both species was similar, segment penetrance exceeding 33% was rarely seen across the large (*n*=285) human cohort, in line with what has been reported previously (Karolchik et al. 2004; Chekaluk et al. 2013). However, the high penetrance of the gains of CFA 13 and 36 and loss of CFA 19 in canine UC resulted in correspondingly high-frequency regions of penetrance on HSA 2, 4, and 8 when presented in their pseudo-human format (Fig. 6b). Copy number aberrations along HSA 2p are evident in cases of human UC at about 20% loss and 4% gain (Fig. 6b (i)). These events are consistent with changes observed in the canine genome. However, in HSA 2q, the extent of the CNAs in regions shared with the dog differs. Along much of the length of HSA 2q, the frequencies of copy number gain and loss are comparable (∼10 %) until 2q32.2, distal to which there is a gradual decline in the frequency of gain and a concomitant increase in frequency of loss, resulting in a gain/loss frequency of 5/20% by the telomeric end of HSA 2q. In the humanized canine data, the proximal region of 2q resembles that observed in human UC, but a 40-Mb region within 2q12–2q32.2 (HSA 2:114–154 Mb) is lost in 77% of canine patients. Adjoining and immediately distal to this region (HSA 2q23.3–32.2) is a 36-Mb (HSA 2:154–190 Mb) span of copy number gain present in ∼83% of cases. This alternating CNA event spans 76 Mb of HSA 2q and is the result of shared conserved chromosome segments with the two highly penetrant CNAs we identified in canine UC: loss of CFA 19 (distal, 33 Mb of the chromosome) and gain of CFA 36.

Low-level CNAs along the length of HSA 4 impact the full length of the chromosome in human UC (∼8% gain and ∼14% loss), as is largely the case with the humanized canine data (Fig. 6b (ii)). However, the canine data demonstrate that the highly penetrant gain of CFA 13 is represented by a 97% gain of HSA 4p14–q13.3 (4:41–75 Mb), while the loss observed at 4q26–q31.21 (4:121–144 Mb) is due to the highly penetrant loss of CFA 19 (proximal, 22 Mb of the chromosome).

In human UC, HSA 8p shows a DNA copy number loss in ∼27% spanning 8p23.3–8p12, which reduced to ∼13% within 8p12–8p11.1 (Fig. 6b (iii)). A subtle gain (4 %) along 8p was noted, with the exception of 8p12– 8p11.1, where the frequency of gain increased to 17 %. A similar pattern was evident in the canine data. In human UC, 8q is subject to a gain in ∼25% of cases at 8q11.1, but this frequency increases along the length of the q-arm so that by 8q22.1, the gain is seen in 34% of cases. The canine data demonstrate CNA frequencies

Author Manuscript Author Manuscript Author Manuscript Author Manuscript

of 10% gain and 4% loss across 8q11–8q22.1, but 97% gain and 0% loss between 8q22.1 and 8q24.3 (the final 40 Mb of 8q). This highly penetrant gain of 8q in humanized data is due to the conserved segment shared with CFA 13.

To quantify the data and facilitate direct comparison of aligned shared genomic CNAs, a higher resolution comparative assessment was conducted using informatics analysis of genomic sequence based on syntenic regions of both genomes. Gains and losses were assessed separately. Shared region lengths were generated from a data-driven approach, ensuring that the novel observations made were compelled by the actual data and not influenced by prior knowledge. The first step of the informatics analysis was to find intersecting regions between the aberration call data and the reference file for both the dog and human, using a threshold of 1 Mb. (Quinlan and Hall 2010). During the subsequent steps of the informatics approach, the shared regions are systematically reduced in size to define those where aberrations are shared between canine and human samples. With this process, a total of 2729 shared copy number gains and 2057 shared copy number losses were identified. For both shared gains and losses, 19 and 22 %, respectively, had a joint-rank probability of ≤0.05. In both cases, approximately 75% of all shared regions were small at <100 kb in size. However, for joint gains, 19% had a length of 100 kb and only 2% were >100 kb. For the losses, ∼1 and 25% of the shared loss regions had a length of 100 and >100 kb, respectively.

Details of the top nine regions of shared rank across both human and canine UC are presented in Table 5 and visualized as concentric Circos plots in Fig. 7. The highest ranked regions of genomic overlap shared between canine and human UC cases included copy number gains of CFA 13/HSA 8 in 97/52% of patients, respectively (Table 5). The specific region of overlap derived from our comparative approach resulted in a segment of HSA 8 that was just 3 kb in size and segment of CFA 13 that was 17.9 kb. This overlapping region had a joint-rank probability of 4.5×10^{-7} and indicates a highly significant role in UC for both dog and human. Within this shared region is the gene polyadenylate-binding protein 1 (*PABPC1*; HSA 8:101,698,044–101,735,037).

Additional significant joint-ranked regions ($p<0.05$) were further evaluated to determine if specific genes associated with CNAs in human UC were also evident in canine UC. Shared gains of *S100A9, S100A8,* and *ID1* and shared loss of *CDKN2A* were identified by our pipeline, supporting this data-driven comparative analysis. In both the data-driven and a priori comparative analyses, the region surrounding HSA 8:101 Mb/CFA 13:54 Mb contained the highest ranked gene in both human and canine UC, PABPC1.

To further assess the potential significance of CNA regions shared between human and canine UC samples, gene ontology (GO) analysis was performed using the Protein Analysis Through Evolutionary Relationships (PANTHER) classification system (Thomas et al. 2003a, b). PANTHER was used to cluster the genes from the ranked list of amplifications and deletions into known GO components. While the number of genes was large, GO analyses highlighted three major gene categories as numerically aberrant in both canine and human cohorts: metabolic processes (GO:008152), cellular processes (GO:0009987), and biological regulation (GO:0065007) (SOM Fig. 1).

Author Manuscript Author Manuscript Author Manuscript Author Manuscript

Comparative pathologic staging

Canine tumors were staged independently by human and veterinary pathologists with very strong agreement (r=0.85) (Table 1), suggesting a high degree of shared histopathologic presentation between canine and human UC. Tumors were staged only to the extent of the biopsy and so in instances where no muscularis was evident, the highest stage possible was T1. When lamina propria was scant or absent, tumors were noted simply as “carcinoma.” When assessed by human pathologists, 25.8% (8/31) of canine UC tumors were classified as stage Tis, with 51.6% (16/31), 16.1% (5/31), and 6.5% (2/31) as T1, T2, and T3, respectively. When assessed by a veterinary pathologists, 48.4% (15/31) were classified as carcinoma, with 29% (9/31), 16.1% (5/31), and 6.5% (2/31) classified as T1, T2, and T3, respectively. Tumors classified as Tis, T1, and carcinoma were assigned as “non-muscle invasive” and the distinct T2 and T3 tumors as “muscle invasive” to facilitate molecular comparison.

Following humanization of canine data, stratification of CNAs by invasive phenotype of tumor stage was performed to identify shared features (Fig. 8). In spite of low numbers of canine cases (which precluded robust statistical analysis), this approach indicted that even at earlier stages, canine tumors have much higher levels of CNAs compared with human tumors. A striking similarity was the presence of a highly recurrent X chromo-some loss (∼50% of cases) in the non-muscle invasive tumors of both human and dog. Shared gains of regions of HSA 1q (CFA 7) and HSA 8q (CFA 13) were also present in >35% of human and canine tumors reported without muscle invasion. In muscle invasive cases, the frequency and size of these chromosomal aberrations increased in both species, along with detection of numerous other CNAs. Additionally, the copy number aberration of chromosome X switches from a copy number loss in ∼50% of non-muscle invasive tumors to a substantial (>50 %) copy number gain in tumors with muscle invasion.

Discussion

Canine UCs exhibit diagnostically relevant copy number aberrations

A major challenge in the management of canine UC is deferred diagnosis. Due to non-specific clinical symptoms mimicking cystitis and the invasive nature of current diagnostic techniques, canine patients with progressive UC often remain undiagnosed for weeks to months (Mutsaers et al. 2003). The use of imaging techniques, such as radiography and ultrasonography, may identify the presence of abnormal growths in the urinary tract but cannot evaluate malignancy. Evaluation of urine sediment by routine cytology can lead to mis-diagnosis; neutrophilic infiltration and degranulation due to bacterial cystitis can cause altered urothelial morphology, mimicking neoplastic cells. Similarly, neo-plastic cells in patients with UC and concurrent bacterial cystitis may elude pathologic detection. As a result, biopsy and histopathologic evaluation is considered the “gold standard” of UC diagnosis (Mutsaers et al. 2003). Biopsy may be performed by surgery, cystoscopy, or traumatic catheterization, all of which are considered invasive procedures. However, disturbance of the primary tumor may result in seeding of malignant epithelial cells throughout the urinary tract (Anderson et al. 1989). The complications associated with

Author Manuscript Author Manuscript Author Manuscript Author Manuscript

tumor seeding, combined with the invasiveness of biopsy techniques, support the need for safer and more efficient diagnostics.

The development of a non-invasive early screening technique to confirm the diagnosis of a UC would provide a means to mitigate the seemingly rapid progression of the disease by facilitating early therapeutic intervention. The propensity of neoplastic cells to be shed into the bladder lumen is one worth exploiting, especially upon examination of the data presented in this study. Three particular CNAs, CFA 13 gain, CFA 36 gain, and CFA 19 loss, were highly recurrent in the canine UC cohort with at least one of these three aberrations detected in 100% of canine patients. Detection of transitional cells in the urine possessing one or more of these aberrations may therefore be considered highly suspicious for UC. Statistical evaluation of our data indicated that, with detection of two or more of these aberrations in cells recovered from a canine urinary tract, the sensitivity and specificity to indicate neoplasia is extremely high (>99 %). Furthermore, the detection of just the two most frequent aneuploidies (gains of CFA 13 and 36) provides an OR of 422.230, a RR of 33.817, and misclassification of 0. The use of FISH as the gold standard of copy number detection and enumeration was shown in this study to be an effective means to identify aberrant cells in urine sediment from dogs that presented with a UC. The use of custom SureFISH probes provided a more reliable, cleaner and effective alternative to conventional genomic (BAC) clone-based FISH probes. This study was based on an evaluation of FFPE and urine specimens from UC confirmed and also grossly healthy canine specimens. To establish true sensitivity and specificity values for a clinically valuable diagnostic assay, similar analyses should be performed using a cohort of canine urine specimens for dogs with non-neoplastic diseases of the urinary tract, including dogs presenting with cystitis due to infection, bladder stones, bladder polyps, and sterile (inflammatory) cystitis.

Canine UC is of comparative value to human medicine

Previous studies have documented HSA 8q as gained in copy number in 37% of human UC patients (Richter et al. 1998). In fact, gain of 8q22 has been identified as the most frequent copy number gain in urothelial carcinomas (Van Duin et al. 2005; Heidenblad et al. 2008) and is generally associated with poor clinical outcome (Chen et al. 2011). Results obtained by combining CNA data from 285 human UC in the present study further supported these reports, with 41% of tumors possessing a gain of 8q. The same aberration is also observed in our canine data set as gain of syntenic CFA 13, albeit with remarkably high frequency at 97% of canine UC cases. We propose that the high prevalence of the HSA 8/CFA 13 gain in UC highlights its importance in both species and simultaneously suggests an evolutionarily conserved molecular pathogenesis in UC tumor development.

Despite the prevalence of the CFA 13 gain in UC, CFA 13 is gained in a number of other canine cancers, including sarcomas and carcinomas (Thomas et al. 2003c, 2014; Angstadt et al. 2011, 2012; Hedan et al. 2011; Poorman et al. 2014). The frequency of this aberration in general canine cancers makes it an unlikely candidate as a single UC-specific marker. Nevertheless, the high prevalence of CFA 13 gain in canine cancer suggests it is likely fundamental to oncogenesis. Comparative analysis of CFA 13 and HSA 8 indicates that if UC indeed shares an evolutionarily conserved mechanism of pathogenesis, genes associated

Author Manuscript Author Manuscript Author Manuscript Author Manuscript

with UC development in both species reside in the proximal half of HSA 8q, the region syntenic with CFA 13.

Using joint-rank probabilities to refine alignment of the canine and human genomes reduced the extent of the shared regions of HSA 8/CFA 13 to a region of the human genome that spans just 3 kb. Within this segment of 8q22.2 is the gene *PABPC1*, whose protein function is to bind the poly-A tail of messenger RNA (mRNA) in the nucleus and shuttle the transcript to the cytoplasm for translation (Eliseeva et al. 2013). PABPC1-associated poly-A tails stimulate translation and stabilize mRNA in the cytoplasm and increased levels of PABPC1 may lead to excessive and oncogenic increases in the mRNA half-lives and thus increased potency of even a normal number of transcripts. Previous studies have shown that *PABPC1* is overexpressed in superficial bladder cancer samples (Chen et al. 2011). Gain of the *PABPC1* locus in superficial and invasive UCs of both canine and human suggests an early and conserved role for the gene in UC progression. In contrast to human UC, the majority of canine tumors are invasive (T1–T4) at the time of diagnosis and thus at the time specimens are available for genomic analyses. This simple yet stark difference in the clinical behavior of canine and human UCs might explain the increased frequency of the aberration in dogs compared with humans, while underlining a potential role of *PABPC1* in tumor progression.

Deletions of HSA 9 are known to be the first genomic alterations associated with human UC development (Simoneau et al. 2000). Specifically, loss of HSA 9q characterizes superficial bladder tumors and becomes less prevalent with increased tumor stage, while gains of HSA 8 become more prevalent (Castillo-Martin et al. 2010). The second most significant shared region according to our joint-rank probability analyses was a region of HSA 9q/CFA 11 that contains *CDKN2A*. This is a widely studied locus in human cancer research as it codes for the p16 tumor suppressor protein, deletion of which has been associated with muscle invasive UC in humans, presumably due to the rapid accumulation of mutations advantageous to tumor progression (Schulz 2006). In fact, the multicolor FISH-based Urovysion® (Abbott Technologies) human bladder cancer diagnostic assay includes *CDKN2A* as one of four regions detected and quantified. Along with focal deletion of *CDKN2A*, a lowered expression of the gene is also observed in human UC samples (Goebell and Knowles 2010; The Cancer Genome Atlas Research Network 2014). The canine UC genome recapitulates the loss of the *CDKN2A* locus at a similar frequency (26% vs. human 38 %), suggesting consequences to expression might also be disrupted in canine UC.

The third- and fourth-ranked regions harbor no apparent coding sequences for genes associated with cancer. The fifth-ranked region was located on HSA 1/CFA 7 (a shared gain) and is immediately flanked by *S100A8* and *S100A9*. When the ranked region was expanded to include the two S100 genes, the aberration penetrance was unchanged. S100A8/9 are two damage-associated molecular pattern proteins (DAMPs) released by monocytes and neutrophils in response to hypoxia, as occurs in a proliferative tumor environment (Bansal et al. 2014). Both S100 proteins have been linked previously to UC development, with overexpression being diagnostic for the disease and higher levels suggestive of higher-grade tumors (Ebbing et al. 2013). Similarly, overexpression of S100A9 is associated with increased proliferation and migration of bladder cancer cell lines

Author Manuscript Author Manuscript Author Manuscript Author Manuscript

(Kim et al. 2011, 2014). The increased frequency of S100 loci gain in dogs (52 %) compared with humans (32 %) may be a reflection of the later time of diagnosis and also may contribute to the more aggressive tumor phenotype seen in canine patients.

Ranked regions with striking interspecies penetrance disparity include loss of HSA 2/CFA 19 and gain of HSA 2/CFA 36 (Table 5, regions 6 and 9). In these regions, copy number aberrations were observed at high frequency in canine UCs, while in humans, the corresponding genomic regions were aberrant only in a small percentage (11 %) of tumors. The discrepancy may be a feature of the differential genome architecture of canine and human karyotypes, in so far as CFA 36 is a small chromosome but is evolutionary conserved as a single 36-Mb segment within the center of HSA 2q (2q23.3–32.2). CFA19 and 36 are juxtaposed on syntenic HSA 2 and are each interrupted by breakpoints which have been clearly documented in human UC at HSA 2q21 and q31, respectively (Fadl-Elmula 2005). Assuming breakpoints are observed in syntenic canine regions, these particular breakpoints would represent fragile sites in CFA 19 and 36 predisposed to duplication, deletion, and translocation. As canine cells evolve to malignancy, rapidly proliferative cells succumb to inherent genomic fragility, resulting in chromosome breaks and copy number aberrations (Richards 2001; Ma et al. 2012; Hosseini et al. 2013).

The prevalence of chromothriptic-like events on CFA 36 confirms suspected fragility of the chromosome. Chromothripsis, a chromosome-shattering phenomenon, leads to extreme genomic rearrangements, deletions, and amplifications within a concentrated chromosomal region (Stephens et al. 2011). In canine UC, 74% of tumors showed distinct chromothriptic-like signatures, most commonly involving CFA 36 (30 %). The amplification of involved regions of CFA 36 interrupted by small regional losses, suggests that, at some point in tumor evolution, CFA 36 sister chromatids were subjected to numerous double-stranded breaks and rejoined imperfectly, leading to the gain of some shattered regions and loss of others. Our results of FISH on neo-plastic urothelial cells support this notion, demonstrating massive amplification of CFA 36 signal within a small nuclear region. Such chromosomal damage may be induced by many means, including mutagenic carcinogens implicated in canine and human UC development. The relatively low frequency of chromothriptic-like events reported in human UC may be attributed to a more compact human genome, composed of 23 chromosome pairs, when compared with the 39 chromosome pairs of the canine karyotype, which leads to increased terminal chromosome surface area available for damage initiation and rejoining.

The aberrant regions on CFA 19 and 36 contain genes of interest to canine UC. The gene *LRP1B* lies within the breakpoint on CFA 19 (Prazeres et al. 2011). LRP1B possesses tumor suppressor function, decreasing the numbers of PDGF and urokinase receptors on the cell membrane and halting external proliferation stimuli. Loss of *LRP1B* is associated with high-grade urothelial carcinoma in humans and may thus be of equal prognostic significance in dogs (Langbein et al. 2002). The fragile site on CFA36 contains the *HOXD* gene cluster and a relevant micro-RNA, miR-10b (Calin et al. 2004). Dysregulated expression of HOX genes leads to increased cell proliferation and neoplastic transformation, whereas upregulation of miR-10b has been associated with invasive and metastatic abilities in numerous carcinomas, including the bladder (Bhatlekar et al. 2014; Xiao et al. 2014).

Author Manuscript Author Manuscript Author Manuscript Author Manuscript

Comparative staging analysis allowed comparison of the molecular landscape throughout tumor progression. Gains of HSA 1 and 8 and loss of X are the most frequent aberrations in non-muscle invasive human tumors, and their syntenic counterparts, CFA 7, 13, and X, are similarly aberrant in canine tumors with absence of muscle invasion. These results reaffirm the importance of HSA 8/CFA 13 gains, in particular, in UC development. Loss of the X chromosome, however, is replaced by a chromosome gain in muscle invasive tumors of both canine and human cases. Previous human UC studies have noted a decrease in the number of tumors demonstrating an X chromosome monosomy and an increase in polysomy with increasing tumor grade (Panani and Roussos 2006). Our results, combined with previous findings regarding tumor grade, suggest the involvement of the X chromosome in UC muscular invasion.

A major limitation to our staging analyses was the superficial nature of canine biopsies. Due to their acquisition via cystoscopy, rarely were all histological layers of the bladder present in the biopsied sample. In these cases, tumors were staged using available layers only. Therefore, it is likely that numerous canine tumors were at a more advanced stage in vivo than we were able to ascertain by biopsy, underrepresenting late-stage tumors and potentially obscuring aberration differences among stages. However, the association with X chromosome copy number status also adds confidence to the histological definitions provided. In future studies, more thorough staging analyses should be performed with more complete canine biopsies. Additionally, the same set of veterinary and human pathologists did not review the human cases, thereby precluding consistency among all human and canine cases

Using PANTHER, the prevalence of genomic aberrations in regions containing critical groups of genes highlights the ways in which chromosomal aberrations contribute to neoplastic transformation. Our analysis adopted an integrative approach that identified genes and pathways that may play a role in UC progression in both canine and human cancers. Using the PANTHER classification system and inputting genome-wide CNAs across both species, we can identify ontological classes that are over- and under-represented in shared genomic regions of canine and human UC samples (SOM Fig. 1). The genes in our analysis are enriched across three major ontological components, including signaling pathways in metabolic processes, cellular processes, and biological regulation. The role of the pathways can now be investigated further by experimental manipulation on both primary UC samples and UC cell lines from both canines and humans. Advances of this nature will lead to new drug discoveries for UC and/or investigation of already available drugs not currently being considered for UC but targeting these same pathways. This type of pathway analyses will be strengthened in the future by combining other comparative genomic data from UC tumors such as sequence mutation, gene expression, and even epigenetic alterations.

Conclusion

The genomic landscape of canine UC is highly aberrant and of enormous diagnostic relevance. The copy number data generated in this study provided the foundations on which to develop a diagnostic assay for canine UC with close to 100% sensitivity and specificity. Furthermore, the non-invasive nature of a free-catch urine-based assay offers an attractive

Author Manuscript Author Manuscript Author Manuscript Author Manuscript

alternative to current options, which will promote earlier detection and thus maximize opportunity for prolonged life. The comparative value of a cross-species approach to cancer gene discovery has been demonstrated for UC with the identification of numerous aberrant genome intervals shared between human and dog. Through direct comparison of canine and human data as well as an informatics approach to highlight the highest ranked changes common to both species, we have demonstrated that dogs and humans share major cytogenomic aberrations that impact signaling pathways. Further evaluation of such genes and pathways as potential therapeutic targets may now be pursued.

Supplementary Material

Refer to Web version on PubMed Central for supplementary material.

Acknowledgments

The canine oaCGH and FISH data generated in this study were funded by the NCSU-CVM Cancer Genomics Fund (MB). SS was supported in part by a Graduate Fellowship from the NCSU Comparative Biomedical Sciences Graduate Program, an NIH-T35 grant, a Triangle Community Foundation award, a George Hitchings New Investigator Award in Health Research, and the NCSU-CVM Cancer Genomics Fund (MB). We gratefully acknowledge support of Skippy Frank Fund for Life Sciences and Translational Research/Rockefeller Philanthropy Advisors (awarded to MB/JS), whose funding supported SR as a Skippy Frank Translational Postdoctoral Fellow. J.D.S. holds the Edward B. Clark, MD Chair in Pediatric Research, and is supported through the Primary Children's Hospital (PCH) Pediatric Cancer Program funded by the Intermountain Healthcare Foundation and the Primary Children's Hospital Foundation. We thank Rachael Thomas for assistance with humanization of canine CGH data and Clint Mason for valuable informatics advice.

References

American Cancer Society. Cancer facts and figures 2014. Society AC; Atlanta: 2014.

American Joint Committee on Cancer. Urinary bladder. In: Greene, F.; Page, D.; Fleming, I., et al., editors. Cancer staging manual. Springer-Verlag; New York: 2002. p. 335-338.

Anderson W, Dunham B, King J, et al. Presumptive subcutaneous transplation of a urinary bladder transitional cell carcinoma of the urinary bladder in a dog. Cornell Vet. 1989; 79:263–266. [PubMed: 2752759]

Angstadt AY, Motsinger-Reif A, Thomas R, et al. Characterization of canine osteosarcoma by array comparative genomic hybridization and RT-qPCR: signatures of genomic imbalance in canine osteosarcoma parallel the human counterpart. Genes Chromosom Cancer. 2011; 50(11):859–874. [PubMed: 21837709]

Angstadt AY, Thayanithy V, Subramanian S, Modiano JF, Breen M. A genome-wide approach to comparative oncology: high-resolution oligonucleotide aCGH of canine and human osteosarcoma pinpoints shared microaberrations. Cancer Genet. 2012; 205(11):572–587. [PubMed: 23137772]

Bansal N, Gupta A, Sankhwar SN, Mahdi AA. Low- and high-grade bladder cancer appraisal via serum-based proteomics approach. Clin Chim Acta. 2014; 436:97–103. [PubMed: 24875752]

Bhatlekar S, Fields JZ, Boman BM. HOX genes and their role in the development of human cancers. J Mol Med. 2014:1432–1440. Electronic.

Cai H, Kumar N, Bagheri H, von Mering C, Robinson M, Baudis M. Chromothripsis-like patterns are recurring but heterogenously distributed features in a survery of 22,347 cancer genome screens. BMC Genomics. 2014; 15:82. [PubMed: 24476156]

Calin GA, Dumitru CS, et al. Human microRNA genes are frequently located at fragile sites and genomic regions involved in cancers. Proc Natl Acad Sci. 2004; 101(9):2999–3004. [PubMed: 14973191]

Castillo-Martin M, Domingo-Domenech J, Karni-Schmidt O, Matos T, Cordon-Cardo C. Molecular pathways of urothelial development and bladder tumorigenesis. Urol Oncol. 2010; 28(4):401–408. [PubMed: 20610278]

Author Manuscript Author Manuscript Author Manuscript Author Manuscript

Chekaluk Y, Wu CL, Rosenberg J, et al. Identification of nine genomic regions of amplification in urothelial carcinoma, correlation with stage, and potential prognostic and therapeutic value. PLoS One. 2013; 8(4):e60927. [PubMed: 23593348]

Chen R, Feng C, Xu Y. Cyclin-dependent kinase-associated protein Cks2 is associated with bladder cancer progression. J Int Med Res. 2011; 39(2):533–540. [PubMed: 21672358]

Development Team R. R: a language and environment for statistical computing. R Foundation for Statistical Computing; Vienna: 2010.

Dhawan D, Ramos-Vara JA, Stewart JC, Zheng R, Knapp DW. Canine invasive transitional cell carcinoma cell lines: in vitro tools to complement a relevant animal model of invasive urinary bladder cancer. Urol Oncol. 2009; 27(3):284–292. [PubMed: 18562222]

Dobson JM. Breed-predispositions to cancer in pedigree dogs. ISRN Veterinary Science. 2013; 2013

Ebbing J, Mathia S, Seibert F, et al. Urinary calprotectin: a new diagnostic marker in urothelial carcinoma of the bladder. World J Urol. 2013:1–8. [PubMed: 23014837]

Eliseeva IA, Lyabin DN, Ovchinnikov LP. Poly(A)-binding proteins: structure, domain organization, and activity regulation. Biochemistry Moscow. 2013; 78(13):1377–1391. [PubMed: 24490729]

Fadl-Elmula I. Chromosomal changes in uroepithelial carcinomas. Cell Chromosom. 2005; 4:1.

Goebell PJ, Knowles MA. Bladder cancer or bladder cancers? Genetically distinct malignant conditions of the urothelium. Urol Oncol. 2010; 28(4):409–428. [PubMed: 20610279]

Hall M, Frank E, Holmes G, Pfahringer B, Reutemann P, Witten IH. The WEKA Data Mining Software: an update. SIGKDD Explorations. 2009; 11

Hedan B, Thomas R, Motsinger-Reif A, et al. Molecular cytogenetic characterization of canine histiocytic sarcoma: a spontaneous model for human histiocytic cancer identifies deletion of tumor suppressor genes and highlights influence of genetic background on tumor behavior. BMC Cancer. 2011 in revision.

Heidenblad M, Lindgren D, Jonson T, et al. Tiling resolution array CGH and high density expression profiling of urothelial carcinomas delineate genomic amplicons and candidate target genes specific for advanced tumors. BMC Med Genomics. 2008; 1:3. [PubMed: 18237450]

Hosseini SA, Horton S, Saldivar JC, et al. Common chromosome fragile sites in human and murine epithelial cells and FHIT/FRA3B loss-induced global genome instability. Genes Chromosom Cancer. 2013; 52(11):1017–1029. [PubMed: 23929738]

Karolchik D, Hinrichs AS, Furey TS, et al. The UCSC Table Browser data retrieval tool. Nucleic Acids Res. 2004; 32(suppl 1):D493–D496. [PubMed: 14681465]

Kim WJ, Kim SK, Jeong P, et al. A four-gene signature predicts disease progression in muscle invasive bladder cancer. Mol Med. 2011; 17(5–6):478–485. [PubMed: 21308147]

Kim WT, Kim J, Yan C, et al. S100A9 and EGFR gene signatures predict disease progression in muscle invasive bladder cancer patients after chemotherapy. Ann Oncol. 2014; 25(5):974–979. [PubMed: 24631944]

Knapp DW, Glickman NW, Denicola DB, Bonney PL, Lin TL, Glickman LT. Naturally-occurring canine transitional cell carcinoma of the urinary bladder A relevant model of human invasive bladder cancer. Urol Oncol. 2000; 5(2):47–59. [PubMed: 21227289]

Knapp D, Ramos-Vara J, Moore G, Dhawan D, Bonney P, Young K. Urinary bladder cancer in dogs, a naturally occurring model for cancer biology and drug development. ILAR J. 2014; 55(1):100–118. [PubMed: 24936033]

Langbein S, Szakacs O, Wilhelm M, et al. Alteration of the LRP1B gene region is associated with high grade of urothelial cancer. Lab Investig. 2002; 82(5):639–643. [PubMed: 12004004]

Ma K, Qiu L, Mrasek K, et al. Common fragile sites: genomic hotspots of DNA damage and carcinogenesis. Int J Mol Sci. 2012; 13(9):11974–11999. [PubMed: 23109895]

Mutsaers AJ, Widmer WR, Knapp DW. Canine transitional cell carcinoma. J Vet Intern Med. 2003; 17(2):136–144. [PubMed: 12683611]

Oliveira PA, Arantes-Rodrigues R, Vasconcelos-Nóbrega C. Animal models of urinary bladder cancer and their application to novel drug discovery. Expert Opin Drug Discov. 2014; 9(5):485–503. [PubMed: 24670247]

Author Manuscript Author Manuscript Author Manuscript Author Manuscript

Panani A, Roussos C. Sex chromosome abnormalities in bladder cancer: Y polysomies are linked to PT1-grade III transitional cell carcinoma. Anticancer Res. 2006; 26(1):319–323. [PubMed: 16475713]

Poorman K, Borst L, Moroff S, et al. Comparative cytogenetic characterization of primary canine melanocytic lesions using array CGH and fluorescence in situ hybridization. Chromosom Res. 2014 in press.

Prazeres H, Torres J, Rodrigues F, Pinto M. Chromosomal, epigenetic and microRNA-mediated inactivation of LRP1B, a modulator of the extracellular envrionemnt of thyroid cancer cells. Oncogene. 2011; 30:1302–1317. [PubMed: 21057533]

Quinlan AR, Hall IM. BEDTools: a flexible suite of utilities for comparing genomic features. Bioinformatics. 2010; 26(6):841–842. [PubMed: 20110278]

Richards R. Fragile and unstable chromosomes in cancer: causes and consequences. Trends Genet. 2001; 17(6):339–345. [PubMed: 11377796]

Richter J, Beffa L, Wagner U, et al. Patterns of chromosomal imbalances in advanced urinary bladder cancer detected by comparative genomic hybridization. Am J Pathol. 1998; 153(5):1615–1621. [PubMed: 9811354]

Sahrief Y, Reich C, Bonar R. Polyploidy in mammalian urothelial cells. Urol Res. 1980; 8:153–161. [PubMed: 7423695]

Schulz W. Understanding urothelial carcinoma through cancer pathways. Int J Cancer. 2006; 119:1513–1518. [PubMed: 16557569]

Shearin AL, Ostrander EA. Leading the way: canine models of genomics and disease. Dis Model Mech. 2010; 3(1–2):27–34. [PubMed: 20075379]

Simoneau M, LaRue H, Aboulkassim T, Meyer F, Moore L, Fradet Y. Chromosome 9 deletions and recurrence of superficial bladder cancer: identification of four regions of prognostic interest. Oncogene. 2000; 19(54):6317–6323. [PubMed: 11175346]

Stephens P, Greenman C, Fu B, Yang F, et al. Massive genomic rearrangement required in a single catastrophic event during cancer development. Cell. 2011; 144(1):27–40. [PubMed: 21215367]

The Cancer Genome Atlas Research Network. Comprehensive molecular characterization of urothelial bladder carcinoma. Nature. 2014; 507(7492):315–322. [PubMed: 24476821]

Thomas PD, Campbell MJ, Kejariwal A, et al. PANTHER: a library of protein families and subfamilies indexed by function. Genome Res. 2003a; 13(9):2129–2141. [PubMed: 12952881]

Thomas PD, Kejariwal A, Campbell MJ, et al. PANTHER: a browsable database of gene products organized by biological function, using curated protein family and subfamily classification. Nucleic Acids Res. 2003b; 31(1):334–341. [PubMed: 12520017]

Thomas R, Smith KC, Ostrander EA, Galibert F, Breen M. Chromosome aberrations in canine multicentric lymphomas detected with comparative genomic hybridisation and a panel of single locus probes. Br J Cancer. 2003c; 89(8):1530–1537. [PubMed: 14562028]

Thomas R, Seiser EL, Motsinger-Reif A, et al. Refining tumor-associated aneuploidy through ‘genomic recoding’ of recurrent DNA copy number aberrations in 150 canine non-Hodgkin lymphomas. Leuk Lymphoma. 2011; 52(7):1321–1335. [PubMed: 21375435]

Thomas R, Borst L, Rotroff D, et al. Genomic profiling reveals extensive heterogeneity in somatic DNA copy number aberrations of canine hemangiosarcoma. Chromosom Res. 2014:1–15.

van Duin M, van Marion R, Vissers K, et al. High-resolution array comparative genomic hybridization of chromosome arm 8q: evaluation of genetic progression markers for prostate cancer. Genes Chromosom Cancer. 2005; 44(4):438–449. [PubMed: 16130124]

Xiao H, Li H, Yu G, et al. MicroRNA-10b promotes migration and invasion through KLF4 and HOXD10 in human bladder cancer. Oncol Rep. 2014; 31(4):1832–1838. [PubMed: 24573354]

Abbreviations

AMADID	Agilent MicroArray Design Identifier
BAC	Bacterial artificial chromosome

Author Manuscript Author Manuscript Author Manuscript Author Manuscript

CDKN2A	Cyclin-dependent kinase inhibitor 2A
CFA	*Canis familiaris* (also used as a prefix to canine chromosome numbers)
CNA	Copy number aberration
DNA	Deoxyribonucleic acid
ECCS	Evolutionarily conserved chromosome segment
FASST2	Fast Adaptive States Segmentation Technique 2
FFPE	Formalin-fixed paraffin embedded
FISH	Fluorescence in situ hybridization
GO	Gene ontology
H&E	Hematoxylin and eosin
HSA	*Homo sapiens* (also used as a prefix to human chromosome numbers)
oaCGH	Oligo-array comparative genomic hybridization
OR	Odds ratio
PANTHER	Protein Analysis Through Evolutionary Relationships
PBS	Phosphate-buffered saline
RR	Relative risk
UC	Urothelial carcinoma
TCC	Transitional cell carcinoma

Author Manuscript Author Manuscript Author Manuscript Author Manuscript

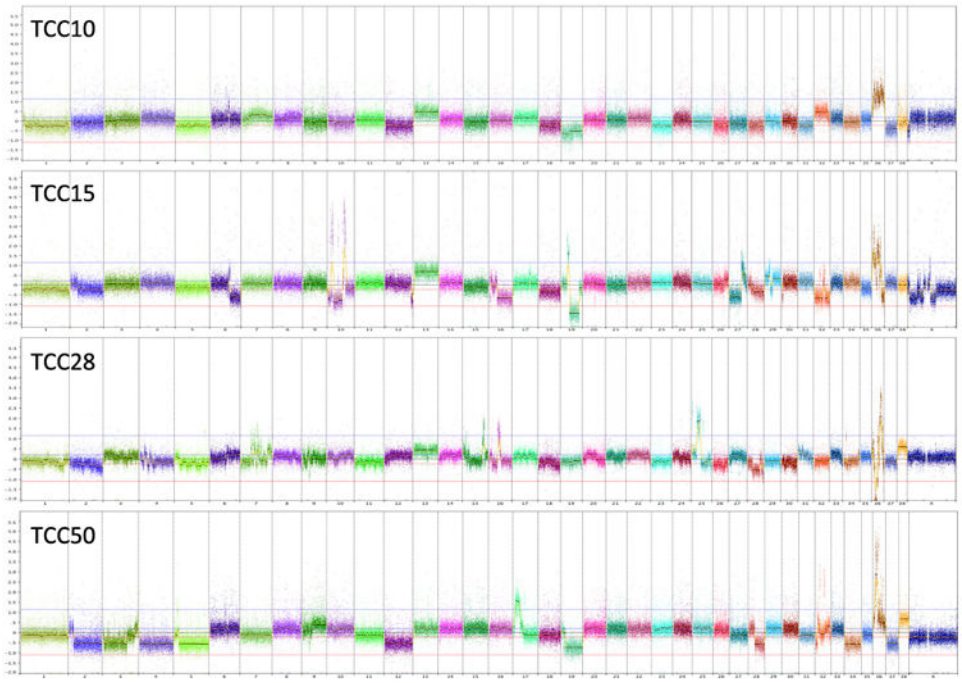

Fig. 1.

Representative oaCGH profiles of four canine UC cases (TCC10, 15, 28, and 50) from the cohort used in the present study. In each case, the oaCGH profiles presents the log2 tumor/reference ratio on the *y*-axis and the genome coordinates of the ∼180,000 probes on the custom array positioned by chromosome location across all 38 canine autosomes and X chromosomes on the *x*-axis. These four cases illustrate the range of CNAs, represented by whole chromosome aneuploidy as well as segmental aneuploidy. Many of the CNAs are suggestive of low-level gain/loss, and there are several regions indicative of amplifications. For example, the extent of copy number gain for regions of CFA 36 is increased from a gain (log2∼1.25) in TCC10 through to a high-level amplification (log2 >4.0) in TCC 15, 28, and 50. Images output from Biodiscovery's Nexus v7.5

Author Manuscript Author Manuscript Author Manuscript Author Manuscript

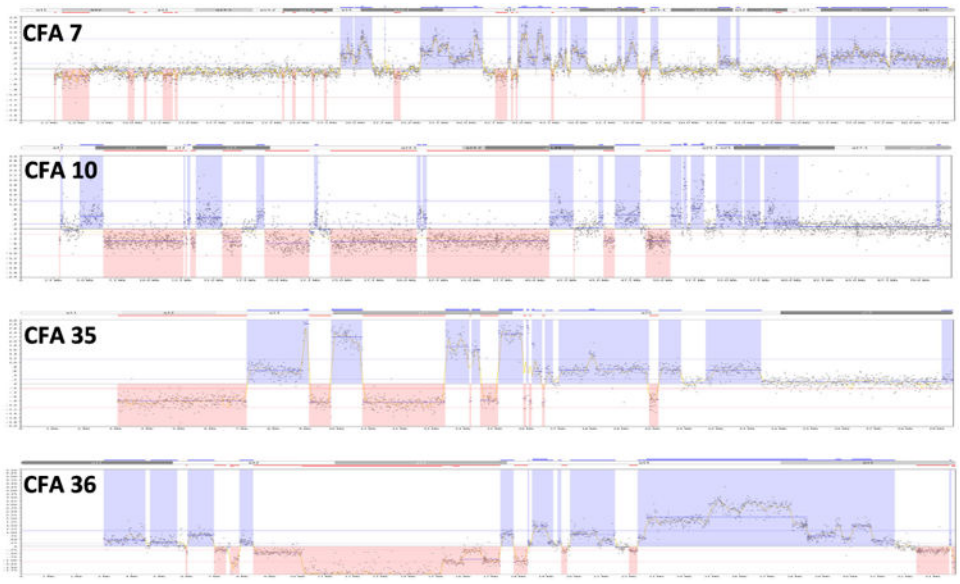

Fig. 2.

Representative chromothriptic-like events detected in canine UC. A chromothriptic-like event was defined as the detection of alternating regions of copy number gain and loss. In each example, regions of copy number gain and loss were determined using the FASST2 algorithm and are *shown with blue* and *red shading*, respectively. The *x*-axis of each of the four chromosomes shown represents the full length of the chromosome, and the *y*-axis represents the log2 ratio of tumor/reference signal

Author Manuscript Author Manuscript Author Manuscript Author Manuscript

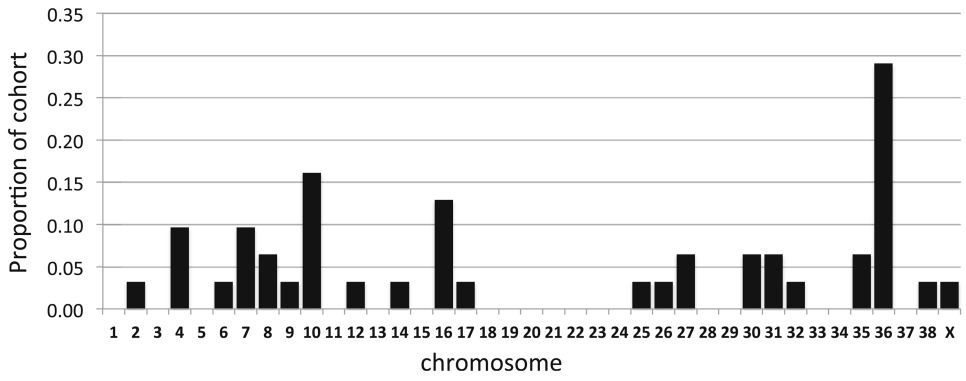

Fig. 3.

Frequency of chromothriptic-like events across the canine genome. Data are based on oaCGH data of 31 cases of canine UC. Each chromosome was evaluated for the presence of chromothriptic-like events and the proportion of canine tumors demonstrating these events on each chromosome was calculated. The proportion of dogs with chromothriptic-like events on CFA 36 was nearly 30 %, suggesting fragility of this particular chromosome

Author Manuscript Author Manuscript Author Manuscript Author Manuscript

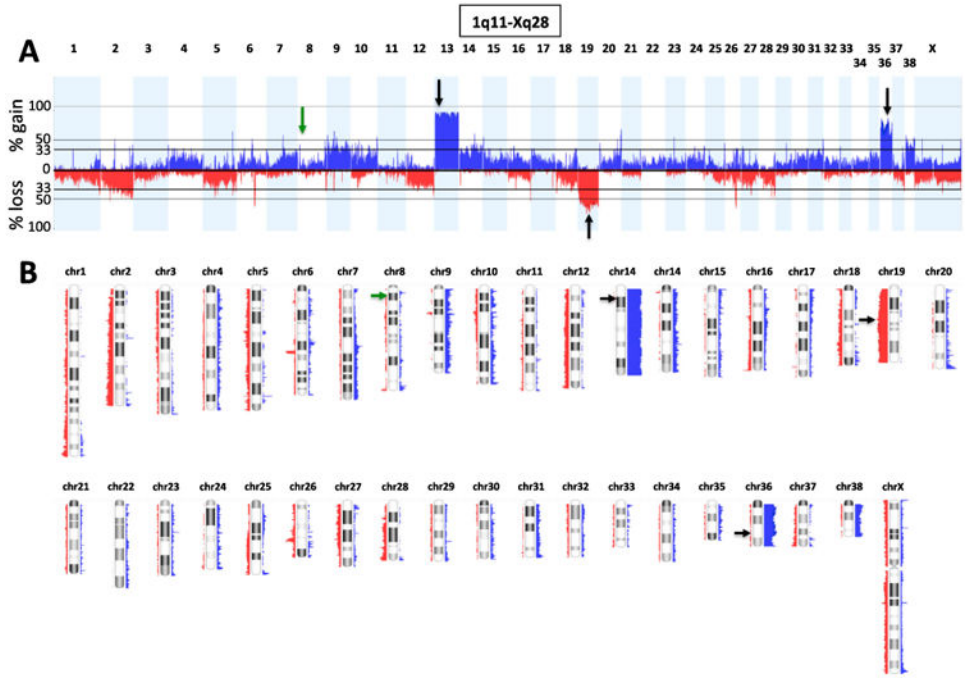

Fig. 4.

Penetrance data of primary canine UC tumors reveal highly recurrent genomic aberrations. **a** Penetrance plot of recurrent CNAs identified within the cohort of 31 canine UC cases. Genomic locations are plotted along the *x*-axis. The *y*-axis indicates the percentage of the corresponding cohort that demonstrated either copy number gain (*shown in blue above the midline*) or loss (*shown in red below the midline*) of the corresponding chromosome region. **b** Canine ideogram indicating regions of CNA. *Blue and red shading to the right and left of each chromosome* indicates the corresponding regions of the chromosomes exhibiting gain and loss, respectively. The *horizontal size of the shading* corresponds with aberration frequency in the population. In (**a**) and (**b**), the highest recurrent unidirectional changes are *shown with arrows* (*black*) on CFA 13, 19, and 36. The *green-arrowed region* of CFA 8 was observed to exhibit a neutral copy number in all 31 cases and so represents a control region

Author Manuscript Author Manuscript Author Manuscript Author Manuscript

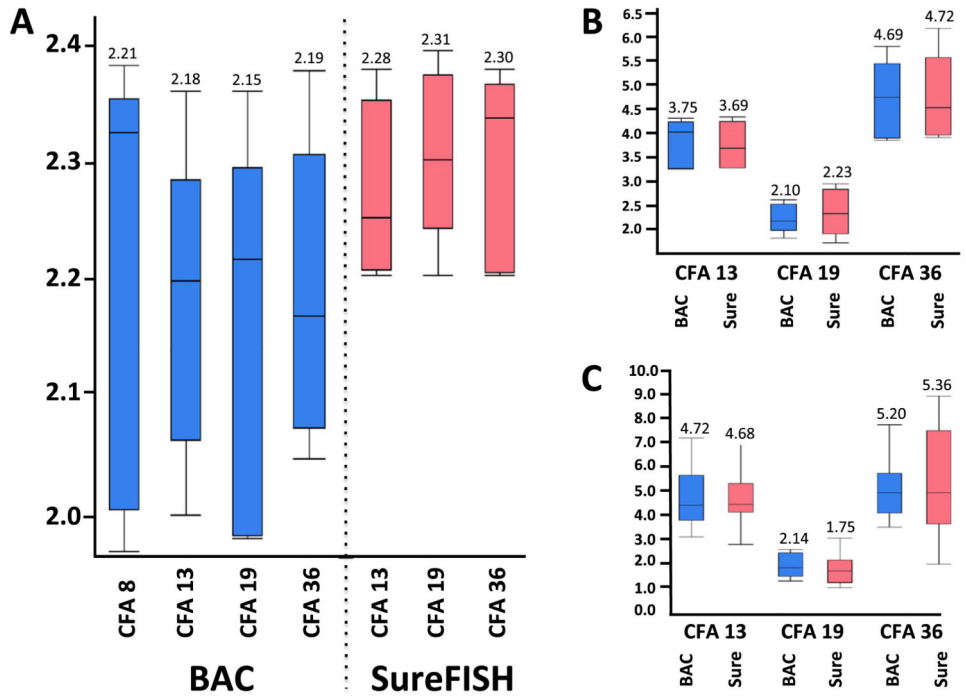

Fig. 5.

BAC and SureFISH methods of copy number detection yield comparable results and elucidate the extent of copy number alteration in canine UC. Distribution of BAC- and SureFISH-derived mean copy number of target regions on CFA 13, 19, and 36 across **a** 5μm FFPE sections of healthy urothelium (*n*=5), **b** 5 μm FFPE sections of confirmed UC (*n*=5), and **c** urine sediment from dogs with confirmed UC (*n*=24). The mean copy number per tumor is *shown on the y-axis*, and the mean value of all patient means is *shown above each box and whisker plot*

Author Manuscript Author Manuscript Author Manuscript Author Manuscript

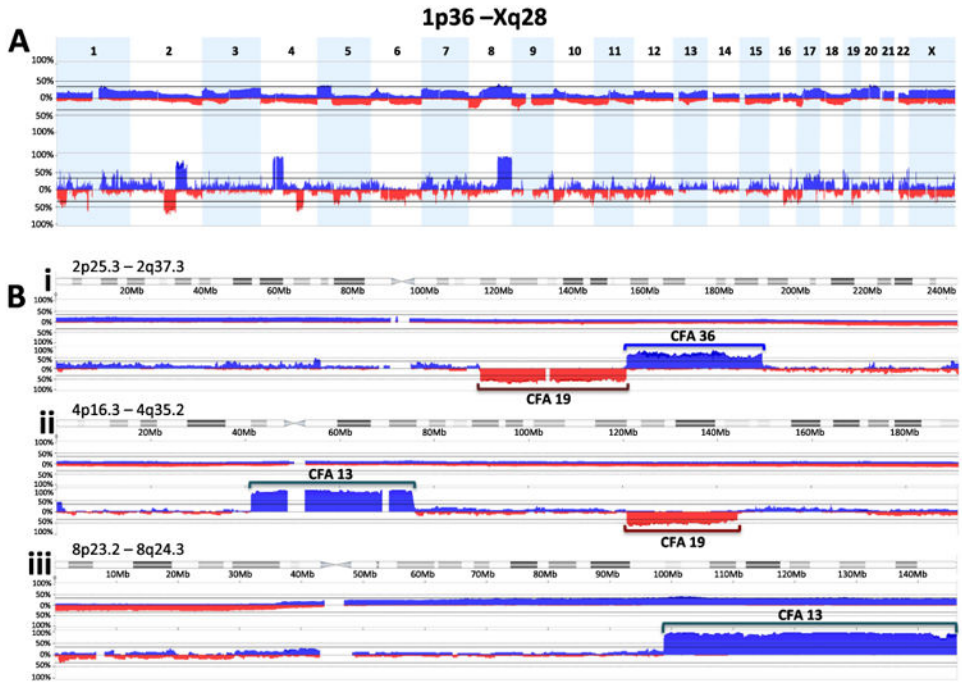

Fig. 6.

Visual comparison of “humanized” canine and human UC oaCGH data. **a** *Top*, penetrance plot of 285 cases of human UC derived from two large public datasets: oaCGH segmented data representing 205 human urothelial tumors produced by the Cancer Genome Atlas (TCGA) and an additional 80 cases of Affymetrix Oncoscan FFPE Express Platform data downloaded from Gene Expression Omnibus (GEO), GSE44323 (Karolchik et al. 2004; Chekaluk et al. 2013). *Bottom*, the penetrance plot of humanized oaCGH data from the 31 canine UC cases generated as part of the present study (canine data shown in Fig. 4a). **b** The high level of penetrance of DNA copy number gain of CFA 13 is reflected along segments of HSA 4 and 8 (*ii*, *iii*). The highly penetrant loss of CFA 19 corresponds to loss of regions of HSA 2 and 4 (*i*, *ii*), and the highly penetrant gain of CFA 36 corresponds to a large region of HSA 2 (*i*), immediately adjacent the region shared with CFA 19

Author Manuscript Author Manuscript Author Manuscript Author Manuscript

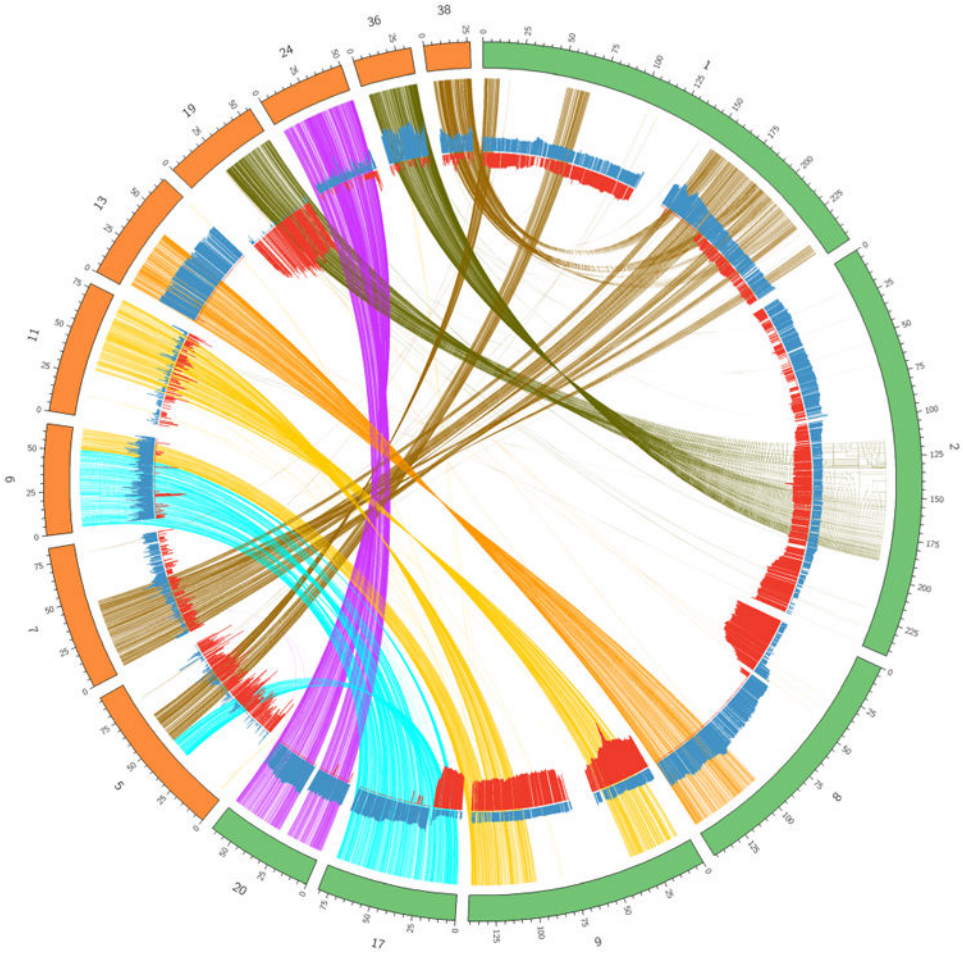

Fig. 7.

Key regions of shared CNA shared between human and canine UC. The nine regions from Table 5 are depicted as a Circos plot. *Orange and green bars in the outer circle* represent canine and human chromosomes, respectively. DNA copy number losses and gains are *shown in red and blue*, respectively, as a histogram on the inner circle. *Color-coded links* display the nine regions of ranked overlap between canine and human chromosomes

Author Manuscript Author Manuscript Author Manuscript Author Manuscript

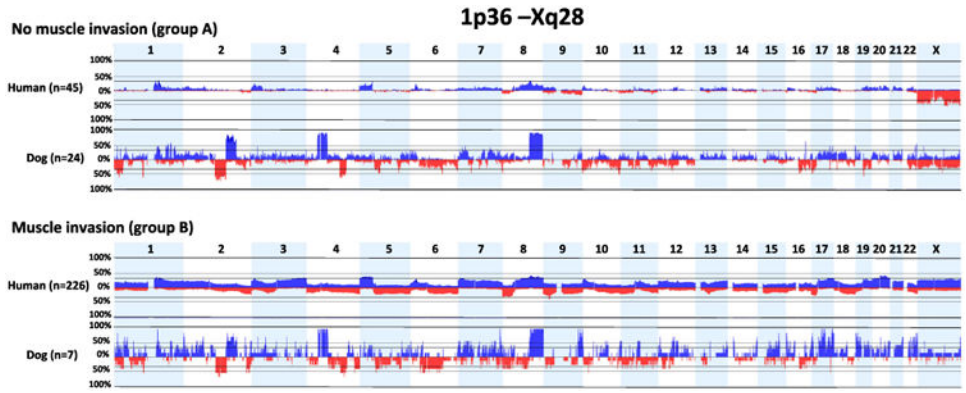

Fig. 8.

Comparison of penetrance of CNAs in human and canine (recoded to human) UC when evaluated by extent of muscle invasion. Based on histopathologic evaluation, cases of canine and human UC were assigned to either group A (no muscle invasion observed) or group B (muscle invasion observed). Following CNA detection, penetrance plots for both human data and humanized canine data were produced in Nexus copy number and presented. Over 50% of the cases with non-muscle invasive tumors in both human and dog are associated with loss of the X chromosome, while >35% of cases with muscle invasion demonstrate a gain of the X chromosome. Human and canine tumors share additional prominent aberrations in non-muscle invasive tumors, notably gains of HSA 1q and HSA 8q. In tumors with muscle invasion, these aberrations, among others, become more prominent

Author Manuscript Author Manuscript Author Manuscript Author Manuscript

Table 1

Canine patient signalment and staging

Case ID	Sample type (biopsy)	Breed	Sex	Vet stage	Human stage	Muscular invasion	Stage group
TCC7	Frozen	Scottish Terrier	FS	Carcinoma	pTis	N	A
TCC8	Frozen	Boxer	MC	pT1	pT1	N	A
TCC9	Frozen	Welsh Corgi	MC	Carcinoma	pT1	N	A
TCC10	Frozen	Mixed Breed	FS	Carcinoma	pT1	N	A
TCC11	Frozen	Treeing Walker Coonhound	FS	Carcinoma	pTis	N	A
TCC12	Frozen	Beagle	MC	pT1	pT1	N	A
TCC13	Frozen	Miniature Schnauzer	FS	Carcinoma	pT1	N	A
TCC15	Frozen	Collie	FS	Carcinoma	pT1	N	A
TCC16	Frozen	Fox Terrier	FS	Carcinoma	pTis	N	A
TCC17	Frozen	Siberian Husky	MC	pT1	pT1	N	A
TCC18	Frozen	Dachshund	FS	Carcinoma	pTis	N	A
TCC19	Frozen	Labrador Retriever	MI	Carcinoma	pT1	N	A
TCC20	Frozen	Jack Russell Terrier	FS	Carcinoma	pTis	N	A
TCC26	Frozen	Beagle	FS	pT1	pT1	N	A
TCC28	Frozen	Beagle	FS	Carcinoma	pT1	N	A
TCC33	FFPE	Scottish Terrier	FS	pT3	pT2	Y	B
TCC34	FFPE	West Highland Terrier	FS	pTis	pTis	N	A
TCC35	FFPE	Dalmation	FS	pT1	pT1	N	A
TCC36	FFPE	German Shepherd	MC	pT2	pT2	Y	B
TCC38	FFPE	Dachshund	MC	pT3	pT3	Y	B
TCC39	FFPE	Keeshond	MC	pT2	pT2	Y	B
TCC40	FFPE	Doberman Pinscher	FS	pT2	pT2	Y	B
TCC42	FFPE	Dachshund	FS	pT2	pT2	Y	B
TCC43	FFPE	Hound	FS	pT1	pT1	N	A
TCC44	FFPE	Corgi	FS	>pT1	>pT1	N	A
TCC45	FFPE	Labrador Retriever	FS	pT1	pT1	N	A
TCC46	FFPE	Miniature Schnauzer	FS	pT2	pT3	Y	B
TCC47	FFPE	Unknown	FS	pTis	>pTis	N	A

Author Manuscript Author Manuscript Author Manuscript Author Manuscript

Case ID	Sample type (biopsy)	Breed	Sex	Vet stage	Human stage	Muscular invasion	Stage group
TCC48	FFPE	Unknown	FS	Carcinoma	pT1	N	A
TCC49	FFPE	Shetland Sheepdog	FS	pT1	At least pT1	N	A
TCC50	FFPE	Basenji	FS	Carcinoma	pTis	N	A

Thirty-one primary UC cases were analyzed in this study. The case identifier, sample type (frozen or FFPE biopsy), breed, and sex are noted for each patient (*F* female, *M* male, *S* spayed, *C* castrated). Stage, as determined by veterinary and human pathologists, is indicated, along with presence of absence of muscle invasion and the consequent analysis group (A vs. B)

Author Manuscript Author Manuscript Author Manuscript Author Manuscript

Table 2

Single-locus probes used to represent the regions of CFA 13, 19, and 36 with the highest recurrence of copy number aberration in canine UC

Chromosome	BAC probes				Sure FISH probes		
	BAC address	Start	Stop	Size (bp)	Start	Stop	Size (bp)
8	122F23	7,984,903	8,129,058	144,155	n/a	n/a	n/a
13	328P06	8,630,922	8,818,498	187,576	8,532,827	8,918,282	385,455
19	122M01	25,119,452	25,264,995	145,543	24,981,989	25,394,047	412,058
36	122F03	23,199,386	23,269,766	70,380	23,037,100	23,421,682	384,582

Clones were selected from the CHORI-82 canine BAC library (www.bacpac.chori.org/library.php?id=253) to represent all three aberrant regions as well as a neutral region on CFA 8. The BAC addresses and clone detail are indicated. Custom SureFISH probes representing overlapping regions of the genome targeted by the BACs were generated in collaboration with Agilent Technologies (Santa Clara, CA) and the details indicated

Chromosome Res. Author manuscript; available in PMC 2015 July 14.

Author Manuscript

Author Manuscript

Author Manuscript

Author Manuscript

Table 3

Frequency of categorical (neutral, loss, or gain) copy number status of the peak unidirectional aberrations on CFA 13, 19, and 31 in cases and controls, determined by analysis of DNA samples isolated form biopsy specimens of 31 cases of confirmed canine TCC and >100 cases of non-malignant cells

Chromosome	Frequency of copy number status		
	Gain (*n*>2; %)	Loss (*n*<2; %)	Neutral (*n*=2; %)
TCC “cases” (*n*=31)			
CFA 13	96.77	0.00	3.23
CFA 19	0.00	77.42	22.58
CFA 36	83.87	0.00	16.13
Normal “controls” (*n*>100)			
CFA 13	0.00	0.00	100.00
CFA 19	0.00	0.00	100.00
CFA 36	0.00	0.00	100.00

The expected copy number of all three of these chromosomes is *n*=2 (neutral), as evident by analysis of cells from healthy dogs. The copy number changes detected for CFA 13, 19, and 36 were unidirectional, with CFA 13 and 36 present as additional copies and CFA 19 with reduced copies

Author Manuscript Author Manuscript Author Manuscript Author Manuscript

Table 4

Summary statistics of the power of each of the three selected regions of CFA 13, 19, and 36 as predictors of the presence of canine UC

Measure	CFA 13			CFA19			CFA36		
	Value	95% confidence interval		Value	95% confidence interval		Value	95% confidence interval	
Relative risk	101	23.044	101	15.286	8.786	9.417	21	10.953	21
Sensitivity	0.968	0.873	0.968	0.774	0.663	0.774	0.839	0.731	0.839
Specificity	1	0.97	1	1	0.966	1	1	0.966	1
Misclassification rate	0.008	0.008	0.053	0.053	0.053	0.106	0.038	0.038	0.089

Author Manuscript Author Manuscript Author Manuscript Author Manuscript

Table 5

Human and canine UC share syntenic regions of copy number aberration

Region number	Human region	Human region size (bp)	Human aberration frequency (%)	Human rank probability	Dog region	Dog region size (bp)	Dog aberration frequency (%)	Dog rank probability	Joint-rank probability	Called aberration
1	hsa8:101720027-101723075	3048	41	3.70E–04	cfal3:5400000-5417899	17,899	97	1.20E-03	4.50E–07	Gain
2	hsa9:21972785-22003700*	30,915	38	5.00E–04	cfal 1:44260998-44276795	15,797	26	0.3	1.30E–04	Loss
3	hsa20:30174575-30174760	185	39	4.10E–03	cfa24:24565372-24570738	5366	68	0.06	2.50E–04	Gain
4	hsal7:5353577-5358463	4886	22	0.04	cfa5:34200000-34217250	17,250	52	0.05	2.20E–03	Loss
5	hsal:153356085-153357875	1790	32	0.05	cfa7:45306965-45330877	23,912	52	0.08	4.30E–03	Gain
6	hsa2:138738449-138740879	2430	11	0.6	cfal9:43939091-44000000	60,909	61	0.02	0.01	Loss
7	hsal7:76151652-76153641	1989	29	0.09	cfa9:4309180-4378991	69,811	35	0.1	0.014	Gain
8	hsal:204501030-204549154	48,124	20	0.43	cfa38:5300000-5312099	12,099	48	0.09	0.04	Gain
9	hsa2:158538468-158550325	11,857	11	0.8	cfa36:6900000-6999021	99,021	84	0.04	0.04	Gain

Regions of shared copy number aberration were determined using human and dog-as-human (humanized) data. For each species, the shared aberrant region on both human and canine chromosomes is listed, as well as the frequency of that aberration in the sample cohort. Overlapping analysis resulted in nine regions with statistical significance ($P<0.05$). Statistical validation was performed by ranking and calculating rank probabilities